Original articles

Comparison study of the conservative Allen–Cahn and the Cahn–Hilliard equations

Dongsun Lee[a], Junseok Kim[b],*

[a] *Department of Mathematical Sciences, Ulsan National Institute Science and Technology, Ulsan 689-798, Republic of Korea*
[b] *Department of Mathematics, Korea University, Seoul 136-713, Republic of Korea*

Highlights

- We compare conservative phase-field models.
- Generation and motion of interface are studied.
- Geometric flows are given and matched to the phase-field equations.
- Modified Allen–Cahn equation is solved using a Lagrange multiplier method.

Abstract

In this paper, a comparison study of conservative Allen–Cahn and Cahn–Hilliard equations is presented. We consider two mass-conservative Allen–Cahn equations and two Cahn–Hilliard equations with constant and variable mobilities. The equations are discretized using finite difference schemes, and discrete systems of the equations are solved using a nonlinear multigrid method. The generation and motion of interface are investigated for the conservative equations. We then present numerical experiments which highlight different dynamics of the four equations.
© 2015 International Association for Mathematics and Computers in Simulation (IMACS). Published by Elsevier B.V. All rights reserved.

1. Introduction

We consider the four conservative phase-field methods on a domain $\Omega \subset \mathbb{R}^d (d = 1, 2, 3)$. The equations of interest are the Cahn–Hilliard and Allen–Cahn equations in the presence of a mass constraint. The phase-field model, an alternative way to approximate the sharp-interface for free surface problems, has been extensively studied [4,13,18,48,71] and successfully applied to describe interfacial motions in chemical and physical modeling of materials and fluid dynamics [1,14,34,54,56,61,77,75,79,80]. Modeling these processes often leads to the conservative equations moving

---
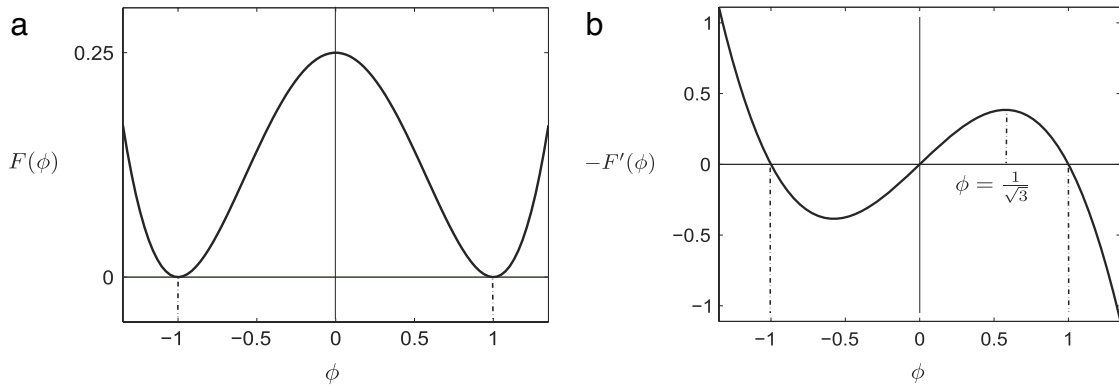
Fig. 1. The forms of (a) the free energy $F(\phi)$ and (b) bistable nonlinearity $-F'(\phi)$.

the interfaces with the velocity that depends on interfacial geometry, while there is no guideline on the selection for the conservative phase-field models.

The objective of this paper is to compare four conservative models for free boundary problems. One is the classical model of conservative Allen–Cahn (CAC1) [17,73] with a nonlocal term $\alpha(t)$:

$$\frac{\partial \phi}{\partial t}(\mathbf{x}, t) = \epsilon^2 \Delta \phi(\mathbf{x}, t) - F'(\phi(\mathbf{x}, t)) + \alpha(t), \quad \mathbf{x} \in \Omega, \ t > 0, \tag{1}$$

where $F(\phi) = 0.25(\phi^2 - 1)^2$ is the free energy per unit volume of homogeneous system of composition, and we write $F'(\phi)$ to indicate the derivative of $F(\phi)$ with respect to ϕ (see Fig. 1(a) and (b)). The term $\alpha(t)$, the time-dependent Lagrange multiplier, which enforces conservation of mass at time t:

$$\int_\Omega \phi(\mathbf{x}, t) \, \mathrm{d}\mathbf{x} = constant.$$

Observe that by the necessary condition for an extremum [43,82] we have $\alpha(t)$ such that

$$\alpha(t) = \frac{\int_\Omega F'(\phi(\mathbf{x}, t)) \, \mathrm{d}\mathbf{x}}{\int_\Omega \, \mathrm{d}\mathbf{x}}.$$

Using the Lagrange multiplier obtained from the costate equation we find the stationary function of the energy functional subject to the integral constraint, which is equivalent to finding the stationary function of a functional with the augmented integrand. Assuming the existence of a stationary solution, we can determine the minimum of system. Thus, applying a gradient method, the costate equation is solved and updated to lead the satisfaction of the stationary condition.

Another is the model of the modified and conservative Allen–Cahn equation with local and nonlocal effects (CAC2) [15], which also imposes the conservation of mass so that

$$\frac{\partial \phi}{\partial t}(\mathbf{x}, t) = \epsilon^2 \Delta \phi(\mathbf{x}, t) - F'(\phi(\mathbf{x}, t)) + \beta(t)k(\phi(\mathbf{x}, t)), \tag{2}$$

where we suppose that $K(\phi) = \phi^3/3 - \phi$ and $K'(\phi)$ indicates the derivative of $K(\phi)$ with respect to ϕ, that is, $K'(\phi) = k(\phi) = 2\sqrt{F(\phi)}$. The term $\beta(t)$ is also the Lagrange multiplier, which is chosen in such a way that

$$\int_\Omega K(\phi) \, \mathrm{d}\mathbf{x} = constant.$$

Similarly, the term $\beta(t)$ for Eq. (2) can be given by the necessary condition

$$\beta(t) = \frac{\int_\Omega F'(\phi(\mathbf{x}, t)) \, \mathrm{d}\mathbf{x}}{\int_\Omega 2\sqrt{F(\phi(\mathbf{x}, t))} \, \mathrm{d}\mathbf{x}}.$$

Next, we consider the constant mobility Cahn–Hilliard (CH) equations [19,21,69],

$$\frac{\partial \phi}{\partial t}(\mathbf{x}, t) = \Delta \mu(\mathbf{x}, t),$$
$$\mu(\mathbf{x}, t) = F'(\phi(\mathbf{x}, t)) - \epsilon^2 \Delta \phi(\mathbf{x}, t),$$

(3)

where μ is called the chemical potential of system. The CH equations arise as a phenomenological model for isothermal phase separation, see the physical and mathematical reviews given in [35,69]. On the other hand, the variable mobility Cahn–Hilliard (mCH) equations [22,36] are used for a thermodynamical reason. The mCH equations read

$$\frac{\partial \phi}{\partial t}(\mathbf{x}, t) = \nabla \cdot [M(\phi) \nabla \mu(\mathbf{x}, t)],$$
$$\mu(\mathbf{x}, t) = F'(\phi(\mathbf{x}, t)) - \epsilon^2 \Delta \phi(\mathbf{x}, t),$$

(4)

where we take a mobility of the form $M(\phi) := 1 - \phi^2$.

The homogeneous Neumann boundary conditions $\mathbf{n} \cdot \nabla \phi = 0$ on $\mathbf{x} \in \partial \Omega$ are assumed for the two mass conservative Allen–Cahn equations, and $\mathbf{n} \cdot \nabla \phi = \mathbf{n} \cdot \nabla \mu = 0$ for the two Cahn–Hilliard equations, respectively. Here $\mathbf{n}$ is the outward normal vector at the domain boundary, and ϵ is a small enough and positive constant. The quantity $\phi(\mathbf{x}, t)$ is defined to be the difference between the mole fractions of binary mixtures (e.g., $\phi(\mathbf{x}, t) = (m_A - m_B)/(m_A + m_B)$ where m_A and m_B are the mole fractions of phases A and B). The variable ϕ is also known as the order parameter, which represents the local state of the entire system. For example, $\phi = 1$ in the one phase and $\phi = -1$ in the other phase. The interface between two phases is defined by $\Gamma_t = \{\mathbf{x} \in \Omega | \phi(\mathbf{x}, t) = 0\}$ at time t.

Stability analyses and error estimates are important for numerical schemes. They were studied, and the numerical tests to verify those were performed in previous works [10,15,87]. We would rather not state all analyses again in our paper, since the main point of our paper is to present the different dynamics among the four equations. But we instead refer to the following papers for more information on stability and error analyses. The numerical schemes were discussed in [90,76,40,58,88,27] for the AC equation, [11,42] for nonlocal AC equation, [29] for the CH equation, and [91,53] for the mCH equation. Moreover, our scheme of the CH and mCH equations are not unconditionally gradient stable [53]. A convex splitting of the free energy functional $F(\phi) = (\phi^2 - 1)^2/4$ yields unconditional energy stability assuring the existence and uniqueness of the solution to the phase-field equations [39,31,60,87].

On the other hand, volume preserving mean curvature flow is also widely used in differential geometry [51,17] and fluids for modeling bubbles [84,59] and the references therein. Mullins–Sekerka problem has been studied in material science. The problem is to describe solidification and liquidation of materials [78]. The surface diffusion flow was proposed by Mullins to describe the motion of the surface grooves at the grain boundaries [68,85].

The remainder of this paper is organized as follows. In Section 2, we consider the properties of the conservative phase-field equations. In Section 3, we present the finite difference discretization of the governing equations and conservation of mass for the discrete equations. In Section 4, we present various numerical results in the early stage and late stage for the evolutionary equations. Finally, we state our conclusions in Section 5.

2. Basic properties of the CAC1, CAC2, CH and mCH equations

In this section we consider the properties of the equations and geometric flows. The geometric flows characterized by sharp-interfaces are the volume preserving mean curvature flow, Mullins–Sekerka flow, and the surface diffusion flow. Evolving interfaces for the geometric flows are assumed to be smooth in a rectangular domain, and meet the boundary at a right angle.

First we consider the CAC1 and CAC2 equations in terms of the volume preserving mean curvature flow. The solution $\phi(\mathbf{x}, t)$ of the CAC1 equation (1) possesses the total mass-conservative property, i.e.,

$$\frac{\mathrm{d}}{\mathrm{d}t} \int_\Omega \phi \, \mathrm{d}\mathbf{x} = \int_\Omega \phi_t \, \mathrm{d}\mathbf{x} = \int_\Omega \left[-F'(\phi) + \epsilon^2 \Delta \phi + \alpha(t) \right] \mathrm{d}\mathbf{x}$$
$$= -\int_\Omega F'(\phi) \, \mathrm{d}\mathbf{x} + \epsilon^2 \int_{\partial \Omega} \mathbf{n} \cdot \nabla \phi \, \mathrm{d}s + \alpha(t) \int_\Omega \mathrm{d}\mathbf{x} = 0.$$

Similarly, the solution $\phi(\mathbf{x}, t)$ of the CAC2 equation (2) has the same property,

$$\frac{d}{dt} \int_\Omega \phi \, d\mathbf{x} = \int_\Omega \phi_t \, d\mathbf{x} = \int_\Omega \left[-F'(\phi) + \epsilon^2 \Delta \phi + 2\beta(t)\sqrt{F(\phi)} \right] d\mathbf{x}$$

$$= -\int_\Omega F'(\phi) \, d\mathbf{x} + \epsilon^2 \int_{\partial \Omega} \mathbf{n} \cdot \nabla \phi \, ds + 2\beta(t) \int_\Omega \sqrt{F(\phi)} \, d\mathbf{x} = 0.$$

Since Eqs. (1) and (2) provide an approximation to the motion by the volume-preserving mean curvature flow [8,15, 17,51,74], the normal velocity V_n at a point p on the interface Γ_τ is given by

$$V_n(p, \tau) = H(p, \tau) - h(\tau).$$

Here τ is a rescaling parameter in time, $\tau = \epsilon t$. In addition, $H(p, \tau)$ stands for the mean curvature of the interface between two phases and $h(\tau)$ is the average of the mean curvature on Γ_τ,

$$h(\tau) = \frac{\int_{\Gamma_\tau} H \, ds}{\int_{\Gamma_\tau} ds},$$

where ds refers to integration with respect to surface measure.

Now, we see that it preserves the volume $Vol(\tau)$ enclosed by Γ_τ, but the surface area $A(\tau)$ decreases until it reaches a stable state for the CAC1 and CAC2 equations. In two-dimensional case, we can replace $Vol(\tau)$ and $A(\tau)$ with $A(\tau)$ and the curve length $L(\tau)$, respectively. To see the preserving volume and decreasing area, we take the derivative of the volume $Vol(\tau)$ and area $A(\tau)$ with respect to the time τ [47,57].

$$\frac{d}{d\tau} Vol(\tau) = \int_{\Gamma_\tau} V_n \, ds = \int_{\Gamma_\tau} (H - h) \, ds = 0,$$

$$\frac{d}{d\tau} A(\tau) = -\int_{\Gamma_\tau} H V_n \, ds = \int_{\Gamma_\tau} (Hh - H^2) \, ds = -\int_{\Gamma_\tau} (h - H)^2 \, ds \le 0,$$

where we used the fact $\int_{\Gamma_\tau} h(h - H) \, ds = h^2 \int_{\Gamma_\tau} ds - h \int_{\Gamma_\tau} H \, ds = 0$. Thus, the motion is driven by volume-preserving and surface area-decreasing curvature flow.

Second, we consider that the solution $\phi(\mathbf{x}, t)$ of the CH equations with the Neumann boundary condition. Also it has mass-conservative property:

$$\frac{d}{dt} \int_\Omega \phi \, d\mathbf{x} = \int_\Omega \phi_t \, d\mathbf{x} = \int_\Omega \Delta \mu \, d\mathbf{x} = \int_{\partial \Omega} \mathbf{n} \cdot \nabla \mu \, ds = 0.$$

Assuming a time scale of $\tau = \epsilon t$, the solution of the CH equations produces the approximation to the Mullins–Sekerka flow or the Hele-Shaw problem ($\Delta \mu = 0$ in $\Omega \backslash \Gamma_\tau$, $\mu = \sigma H$, σ is a positive constant) [4,23,24,33,38,72] and references therein. Note that the relationship between the Mullins–Sekerka model and the Cahn–Hilliard equations with constant mobility was formally derived by Pego [72]. In the literature the Mullins–Sekerka flow can be seen as the Hele-Shaw problem. The normal velocity V_n is followed by the Mullins–Sekerka flow:

$$V_n = \left[\frac{\partial \mu}{\partial n} \right]_{\Gamma_\tau} = \frac{\partial \mu^+}{\partial n} - \frac{\partial \mu^-}{\partial n},$$

where μ^+ and μ^- are the restriction of μ on Ω_t^+ and Ω_t^-, respectively. Using Gauss' theorem, the time derivative of the volume and surface area are given by

$$\frac{d}{d\tau} Vol(\tau) = -\int_{\Gamma_\tau} V \, ds = \int_{\Gamma_\tau} \left[\frac{\partial \mu}{\partial n} \right]_{\Gamma_\tau} ds$$

$$= \int_{\partial \Omega} \frac{\partial \mu}{\partial n} \, ds - \int_{\Omega \backslash \Gamma_\tau} \Delta \mu \, d\mathbf{x} = 0,$$

$$\frac{d}{d\tau} A(\tau) = -\int_{\Gamma_\tau} H V_n \, ds = \int_{\Gamma_\tau} \mu \left[\frac{\partial \mu}{\partial n} \right]_{\Gamma_\tau} ds = -\int_{\Omega \backslash \Gamma_\tau} |\nabla \mu|^2 \, d\mathbf{x} \le 0.$$

Third, the mCH equations also give mass-conserving property:

$$\frac{d}{dt}\int_\Omega \phi\,d\mathbf{x} = \int_\Omega \phi_t\,d\mathbf{x} = \int_\Omega \nabla\cdot(M(\phi)\nabla\mu)\,d\mathbf{x} = \int_{\partial\Omega} M(\phi)\mathbf{n}\cdot\nabla\mu\,\,\mathrm{d}s = 0.$$

Unlike the constant mobility CH equations, Eq. (4) can be viewed as motion by the surface diffusion flow. If the mobility is $M(\phi) = 1 - \phi^2$, Cahn, Elliot and Novick-Cohen [20] showed that the equations follow the surface diffusion flow. This motion also preserves the volume of system, but its area is decreasing. Assuming a time scale of $\tau = \epsilon t$, the zero-level set of the solution to the mCH equations produces the surface diffusion flow [20,37,66]. The normal velocity V_n is followed by the surface diffusion flow:

$$V_n(p,\tau) = -\Delta_s H(p,\tau),$$

where Δ_s is the surface Laplacian, which is also defined as $\Delta_s = \nabla_s \cdot \nabla_s$ and ∇_s is surface gradient. The time derivatives of the volume and surface area are given by

$$\frac{d}{d\tau}Vol(\tau) = \int_{\Gamma_\tau} V_n\,\mathrm{d}s = -\int_{\Gamma_\tau} \Delta_s H\,\mathrm{d}s = 0,$$

$$\frac{d}{d\tau}A(\tau) = -\int_{\Gamma_\tau} HV_n\,\mathrm{d}s = \int_{\Gamma_\tau} H\Delta_s H\,\mathrm{d}s = -\int_{\Gamma_\tau} |\nabla_s H|^2\,\mathrm{d}s \le 0.$$

3. Numerical schemes

In this section, we describe finite difference discretizations for solving CAC1, CAC2, CH and mCH equations, respectively. For simplicity of exposition, we shall discretize the equations in two-dimensional space. Let a computational domain $\Omega = (a,b) \times (c,d)$ be partitioned into a uniform mesh with mesh spacing h. Let $h = (b-a)/N_x = (d-c)/N_y$ be the spatial step size. The center of each cell, Ω_{ij}, is located at $\mathbf{x}_{ij} = (x_i, y_j) = (a + (i - 0.5)h, c + (j - 0.5)h)$ for $i = 1, \ldots, N_x$ and $j = 1, \ldots, N_y$. Here, N_x and N_y are the numbers of cells in x- and y-directions, respectively. Let ϕ_{ij}^n and μ_{ij}^n be approximations of $\phi(x_i, y_j, n\Delta t)$ and $\mu(x_i, y_j, n\Delta t)$, where $\Delta t = T/N_t$ is the temporal step, T is the final time, and N_t is the total number of temporal steps.

3.1. Numerical algorithms for the CAC1 and CAC2 equations

First, let us start with definitions of differential operators and inner products. The discrete differential operators are defined by

$$D_x\phi_{i+1/2,j} = \frac{\phi_{i+1,j} - \phi_{i-1,j}}{h}, \qquad D_y\phi_{i,j+1/2} = \frac{\phi_{i,j+1} - \phi_{i,j-1}}{h}.$$

Next we define the discrete l^2 inner product by

$$(\phi, \psi)_h = h^2 \sum_{i=1}^{Nx}\sum_{j=1}^{Ny} \phi_{ij}\psi_{ij},$$

$$(\nabla_d\phi, \nabla_d\psi)_e = h^2\left(\sum_{i=1}^{Nx}\sum_{j=1}^{Ny} D_x\phi_{i+1/2,j}D_x\psi_{i+1/2j,} + \sum_{i=1}^{Nx}\sum_{j=1}^{Ny} D_y\phi_{i,j+1/2}D_y\psi_{i,j+1/2}\right),$$

where we use the notation $\nabla_d\phi_{i,j} = (D_x\phi_{i+1/2,j}, D_y\phi_{i,j+1/2})$. Using this, we also define the discrete Laplacian ($\Delta_d\phi_{i,j} = \nabla_d \cdot \nabla_d\phi_{i,j}$) by

$$\Delta_d\phi_{i,j} = \frac{D_x\phi_{i+1/2,j} - D_x\phi_{i-1/2,j}}{h} + \frac{D_y\phi_{i,j+1/2} - D_y\phi_{i,j-1/2}}{h}.$$

Imposing the zero Neumann boundary condition, we require that

$$D_x\phi_{i-\frac{1}{2},j} = 0 \quad \text{for } i = 1, \qquad D_x\phi_{i+\frac{1}{2},j} = 0 \quad \text{for } i = N_x,$$

$$D_y\phi_{i,j-\frac{1}{2}} = 0 \quad \text{for } j = 1, \qquad D_y\phi_{i,j+\frac{1}{2}} = 0 \quad \text{for } j = N_x.$$

In this subsection, we use the finite difference, and show the numerical schemes and discrete version of mass-conservation property. First, we consider the CAC1 equation:

$$\phi_t = \epsilon^2 \Delta\phi - F'(\phi) + \alpha(t). \tag{5}$$

As first step, we solve Eq. (5) by a semi-implicit time and centered difference scheme:

$$\frac{\phi_{ij}^* - \phi_{ij}^n}{\delta t} = \frac{\epsilon^2}{2}\left(\Delta_d\phi_{ij}^* + \Delta_d\phi_{ij}^n\right) - F'(\phi_{ij}^*) \tag{6}$$

where $F'(\phi_{ij}^*)$ is nonlinear with respect to ϕ_{ij}^*, and we linearize it at ϕ_{ij}^n:

$$F'(\phi_{ij}^*) = F'(\phi_{ij}^n) + \frac{dF'(\phi_{ij}^*)}{d\phi}(\phi_{ij}^* - \phi_{ij}^n).$$

Then we solve Eq. (7) with the Lagrange multiplier α^*

$$\frac{\phi_{ij}^{n+1} - \phi_{ij}^*}{\delta t} = \alpha^*, \tag{7}$$

where $\alpha^* = \sum_{i=1}^{N_x}\sum_{j=1}^{N_y} F'(\phi_{ij}^*)/(N_x N_y)$.

We now show that the scheme is mass-conserving. Suppose that ϕ^n is a solution of (5). The following equations are discrete version of Eqs. (6) and (7):

$$(\phi^*, 1)_h = (\phi^n, 1)_h + \frac{\delta t}{2}(\epsilon^2\Delta_d\phi^*, 1)_h + \frac{\delta t}{2}(\epsilon^2\Delta_d\phi^n, 1)_h - \delta t(F'(\phi^*), 1)_h \tag{8}$$

$$(\phi^{n+1}, 1)_h = (\phi^*, 1)_h + \delta t(\alpha^*, 1)_h. \tag{9}$$

If we sum up Eqs. (8) and (9), then

$$(\phi^{n+1}, 1)_h = (\phi^n, 1)_h + \frac{\delta t}{2}(\epsilon^2\Delta_d\phi^*, 1)_h + \frac{\delta t}{2}(\epsilon^2\Delta_d\phi^n, 1)_h - \delta t(F'(\phi^*), 1)_h + \delta t(\alpha^*, 1)_h$$

$$= (\phi^n, 1)_h + \frac{\delta t}{2}(\epsilon^2\nabla_d\phi^{n+1}, \nabla_d 1)_h + \frac{\delta t}{2}(\epsilon^2\nabla_d\phi^{n+1}, \nabla_d 1)_h - \delta t(F'(\phi^*), 1)_h + \delta t(\alpha^*, 1)_h$$

where summation by parts is used. Accordingly, we obtain from the definition of (α^*):

$$(\phi^{n+1}, 1)_h = (\phi^n, 1)_h - \delta t(F'(\phi^*), 1)_h + \delta t(F'(\phi^*), 1)_h$$

$$= (\phi^n, 1)_h.$$

This gives that the updated numerical solutions ϕ^{n+1}, $n = 1, \ldots, N_t$ follow the mass-conservative property, i.e., $\sum_{i=1}^{N_x}\sum_{j=1}^{N_y}\phi_{ij}^{n+1} = \sum_{i=1}^{N_x}\sum_{j=1}^{N_y}\phi_{ij}^0$.

For the CAC2 equation, we have

$$\phi_t = \epsilon^2\Delta\phi - F'(\phi) + \beta(t)2\sqrt{F(\phi)}. \tag{10}$$

As before, we can decouple Eq. (10) with

$$\frac{\phi_{ij}^* - \phi_{ij}^n}{\delta t} = \frac{\epsilon^2}{2}\left(\Delta_d\phi_{ij}^* + \Delta_d\phi_{ij}^n\right) + F'(\phi_{ij}^*), \tag{11}$$

and

$$\frac{\phi_{ij}^{n+1} - \phi_{ij}^*}{\delta t} = 2\sqrt{F(\phi_{ij}^n)}\beta^*. \tag{12}$$

The only difference from the previous one is in that the nonlocal term used by

$$\beta^* = \sum_{l=1}^{N_x}\sum_{k=1}^{N_y}(F'(\phi_{lk}^*)) \Big/ \sum_{l=1}^{N_x}\sum_{k=1}^{N_y}2\sqrt{F(\phi_{lk}^n)}$$

instead of α^*. If ϕ^n is the solution of (10), then we have $\sum_{i=1}^{N_x}\sum_{j=1}^{N_y}\phi_{ij}^{n+1} = \sum_{i=1}^{N_x}\sum_{j=1}^{N_y}\phi_{ij}^0$. To see this, we have two discretized equations of (11) and (12):

$$(\phi^*, 1)_h = (\phi^n, 1)_h + \frac{\delta t}{2}(\epsilon^2\Delta_d\phi^*, 1)_h + \frac{\delta t}{2}(\epsilon^2\Delta_d\phi^n, 1)_h - \delta t(F'(\phi^*), 1)_h \tag{13}$$

$$(\phi^{n+1}, 1)_h = (\phi^*, 1)_h + \delta t(\beta^*2\sqrt{F(\phi^n)}, 1)_h. \tag{14}$$

If we sum up Eqs. (13) and (14), then

$$(\phi^{n+1}, 1)_h = (\phi^n, 1)_h + \frac{\delta t}{2}(\epsilon^2\Delta_d\phi^*, 1)_h + \frac{\delta t}{2}(\epsilon^2\Delta_d\phi^n, 1)_h - \delta t(F'(\phi^*), 1)_h + \delta t(\beta^*2\sqrt{F(\phi^n)}, 1)_h$$

$$= (\phi^n, 1)_h + \frac{\delta t}{2}(\epsilon^2\nabla_d\phi^*, \nabla_d 1)_h + \frac{\delta t}{2}(\epsilon^2\nabla_d\phi^n, \nabla_d 1)_h - \delta t(F'(\phi^*), 1)_h + \delta t(\beta^*2\sqrt{F(\phi^n)}, 1)_h$$

where we have the Lagrange multiplier β^*. That is, we obtain

$$(\phi^{n+1}, 1)_h = (\phi^n, 1)_h - \delta t[(F'(\phi^*), 1)_h] + \delta t\left[\frac{(F'(\phi^*), 1)_h}{(2\sqrt{F(\phi^n)}, 1)_h}(2\sqrt{F(\phi^n)}, 1)_h\right]$$

$$= (\phi^n, 1)_h.$$

The updated numerical solution ϕ^{n+1} also satisfies the mass-conservative property.

3.2. Numerical algorithm for the CH equation

We treat the CH equations (3) as a system of second-order equations in space, which yields the following discrete approximation:

$$\frac{\phi_{ij}^{n+1} - \phi_{ij}^n}{\Delta t} = \Delta_d\mu_{ij}^*,$$
$$\mu_{ij}^* = F'(\phi_{ij}^*) - \frac{\epsilon^2}{2}\Delta_d(\phi_{ij}^{n+1} + \phi_{ij}^n). \tag{15}$$

The nonlinear system of Eqs. (15) is solved efficiently using a nonlinear multigrid method [16,56,81,83]. Now we show that the numerical scheme is mass-conserving as below:

$$(\phi^{n+1}, 1)_h = (\phi^n, 1)_h + \delta t(\Delta_d\mu^*, 1)_h = (\phi^n, 1)_h - \delta t(\nabla_d\mu^*, \nabla_d 1)_e$$
$$= (\phi^n, 1)_h.$$

Therefore we have the mass-conservative property for the CH equations, $\sum_{i=1}^{N_x}\sum_{j=1}^{N_y}\phi_{ij}^{n+1} = \sum_{i=1}^{N_x}\sum_{j=1}^{N_y}\phi_{ij}^n$. We note that convergence and mass-conservative property of the discrete system are found in [56].

3.3. Numerical algorithm for the mCH equation

We consider the variable mobility CH equations (4). A semi-implicit time and centered difference scheme of the mCH equations is given by

$$\frac{\phi_{ij}^{n+1} - \phi_{ij}^n}{\Delta t} = \nabla_d \cdot [M(\phi)^{n+\frac{1}{2}}\nabla_d\mu_{ij}^{n+\frac{1}{2}}],$$
$$\mu_{ij}^{n+\frac{1}{2}} = \frac{1}{2}(F'(\phi_{ij}^{n+1}) + F'(\phi_{ij}^n)) - \frac{\epsilon^2}{2}\Delta_d(\phi_{ij}^{n+1} + \phi_{ij}^n). \tag{16}$$

The nonlinear system of Eqs. (16) is solved similar to the CH equations using a nonlinear multigrid method. The mass-conservation of Eqs. (16) was proved in [53] as below:

$$(\phi^{n+1}, 1)_h = (\phi^n, 1)_h + \delta t(\nabla_d \cdot (M\nabla_d\mu^{n+\frac{1}{2}}), 1)_h$$
$$= (\phi^{n+1}, 1)_h - \delta t(M\nabla_d\mu^{1+\frac{1}{2}}, \nabla_d 1)_e = (\phi^n, 1)_h.$$
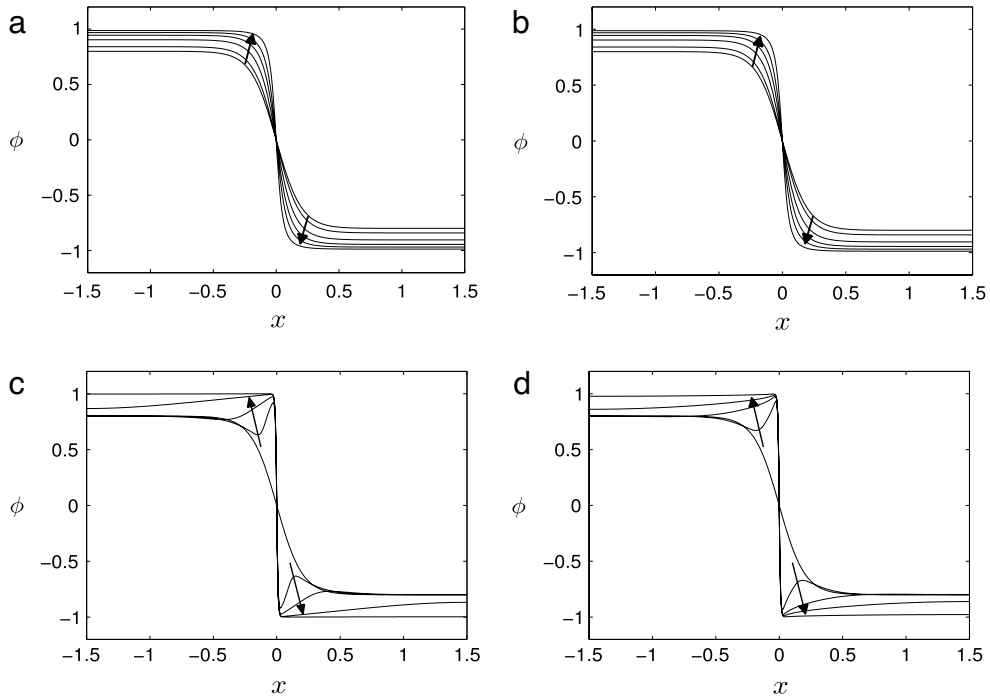
Fig. 2. Equilibrium (a) CAC1 and (b) CAC2 (c) CH, and (d) mCH solutions of an initial concentration $\phi(x, 0) = -0.8\tanh(5x)$.

4. Evolutions under the CAC1, CAC2, CH and mCH equations

We consider that the evolution under the equations, which undergoes two stages called generation of interface and motion of interface. The aim of this section is to show the differences of four equations for these two stages. Numerical tests are presented for generation of interface in one-dimensional space, and then we compare several examples such as two-circles case, small circle case, preserving the convexity in convex case, and a non-convex case in terms of the geometric flows.

Note that the concentration field across the interfacial region varies from -0.9945 to 0.9945 where a distance of approximately $2\sqrt{2}\epsilon \tanh^{-1}(0.9945)$ for the numerical tests. Therefore, if we want this value to be approximately m grid points, the ϵ value needs to be taken as follows: $\epsilon_m = hm/[2\sqrt{2}\tanh^{-1}(0.9945)]$.

4.1. Generation of interface

First we compare solutions of the CAC1, CAC2, CH and mCH equations for the early stage or spinodal decomposition. The generation of the interface is characterized by transition layers between two phases with an equilibrium profile $\phi_\epsilon(x) = \tanh\left(x/(\sqrt{2}\epsilon)\right)$, thus we have the globally stable transition layer solution [12,15]. Fig. 2 shows evolutions of an initial concentration $\phi(x, 0) = -0.8\tanh(5x)$ on domain $\Omega = (-1.5, 1.5)$. In this case, global and transition layer solutions of CAC1, CAC2, CH, and mCH equations are obtained in common.

Now we see the different aspect of the equations. In this early stage, the harmonic terms $\epsilon^2 \Delta \phi$ in Eqs. (1) and (2) are negligible since they have small effects compared to $F'(\phi)$. In particular, it tends ± 1 depending on the sign of the initial profile. Ignoring small ϵ^2 term, we rewrite the CAC1 equation as

$$\phi_t = -F'(\phi) + \alpha(t).$$

Similarly, we rewrite the CAC2 equation as

$$\phi_t = -F'(\phi) + \beta(t)2\sqrt{F(\phi)}.$$

Since we have the Lagrange multipliers $\alpha(t)$ and $\beta(t)2\sqrt{F(\phi)}$, which vanish in equilibrium, the solutions $|\phi| \leq 1$ are obtained from direct consequence of the profile of $-F'(\phi)$ (see Fig. 1(b)).
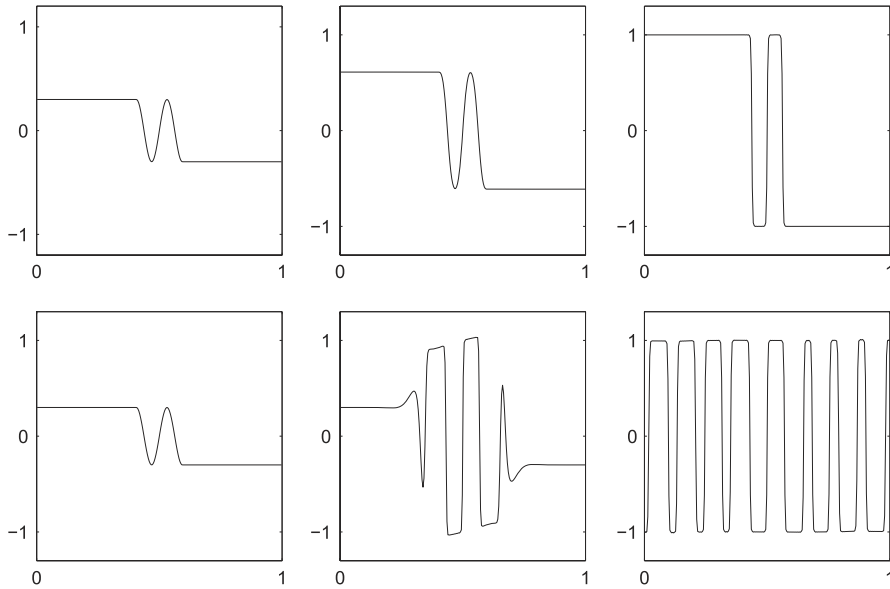
Fig. 3. Evolutions under the CAC1 (top row) and CH (bottom row) equations. Figures are ordered from left to right according the progress in time. The horizontal axis is in space x and the vertical axis is in order parameter ϕ.

Unlike the evolution under the CAC1 and CAC2 equations (see Fig. 3 first row), which depends on initial profile, the CH and mCH have different interface formations in the early stage. For the CH equation, we assume that $\phi(x) = \bar{\phi} + \tilde{\phi}$. Here we suppose that $\tilde{\phi}(x)$ represents a small perturbation from spatial uniformly $\bar{\phi}$, then linearizing the CH equations (3) about $\bar{\phi}$ gives

$$\tilde{\phi}_t = (3\bar{\phi}^2 - 1)\phi_{xx}. \tag{17}$$

Seeing that for $(3\bar{\phi}^2 - 1) > 0$, we have the diffusion equation with Neumann boundary conditions. For $(3\bar{\phi}^2 - 1) < 0$, i.e. $\bar{\phi}$ is in spinodal interval, we however have the backward diffusion equation. In this case, Eq. (17) is ill-posed, and needs the higher order terms proportional to ϵ^2. This term provides the regularity of the CH equations. Therefore we perform the linear analysis with the regularizing term. Assuming $\bar{\phi}$ is in the spinodal region, we have $\gamma^2 := -F''(\bar{\phi}) > 0$. The linearized form is given by

$$\begin{aligned} \phi_t &= -\epsilon^2 \phi_{xxxx} - \gamma^2 \phi_{xx}, \quad x \in \Omega(0,1) \\ \phi_x &= \phi_{xxx} = 0 \quad x \in \partial\Omega(0,1). \end{aligned} \tag{18}$$

Since the eigenfunctions of the linear operator are subject to the boundary conditions, we have

$$\{\cos n\pi x : n = 1, 2, \ldots\}.$$

Plugging $\phi = a_n \cos n\pi x$ into Eq. (18), we have

$$a_n' \cos n\pi x = -\epsilon^2 (n\pi)^4 a_n \cos n\pi x + \gamma^2 (n\pi)^2 a_n \cos n\pi x,$$

where a_n is a function of t, and $a_n' = (n\pi)^2 [\gamma^2 - \epsilon^2 (n\pi)^2] a_n$. Thus, we get

$$a_n(t) = a_n(0) \exp(\lambda_n t),$$

where $\lambda_n = (n\pi)^2 [\gamma^2 - \epsilon^2 (n\pi)^2]$, i.e., $a_n(t)$ and λ_n are the eigenfunctions and eigenvalues. For $0 < n < \beta/(\epsilon\pi)$ and λ_n, the corresponding Fourier modes grow as time progresses in Eq. (18). Therefore, the solutions evolve relatively fast and become nearly periodic (see Fig. 3 bottom row).

For the mCH equations, letting $\phi(x, t) = \bar{\phi} + \phi(\tilde{x}, t)$, the mCH equations (4) give

$$\tilde{\phi}_t = \{(1 - \phi^2)[-\epsilon^2 \phi_{xx} - \bar{\phi} - \tilde{\phi} + (\bar{\phi} + \tilde{\phi})^3]_x\}_x. \tag{19}$$

Assuming $\tilde{\phi}$ to be small, we neglect nonlinear terms. Linearizing equation (19) about $\bar{\phi}$ gives

$$\tilde{\phi}_t = [1 - \bar{\phi}^2](3\bar{\phi}^2 - 1)\phi_{xx}.$$

If the mobility is positive $1 - \bar{\phi}^2 > 0$, then it is the backwards diffusion equation in the spinodal interval. Therefore, we have the periodic solutions of linear instability, like the CH equations' solutions. A more detailed explanation of such behaviors are found in [49,50]. We also refer to [2,3] on the generation of interface of the CAC1 and CAC2 equations, global solution of the CH equations [6], and see [7,9,46,63,70] on the spinodal decomposition and linear analysis.

4.2. Motion of interface

Previously we observe that the solutions ϕ of the four equations develop transition layers in the early stage. The present subsection is to show the motion of interface, once the transition layer is formed. From now on we assume that the profile of solutions ϕ^ϵ already has transition layers depending on ϵ.

We now consider theoretically and numerically that the internal transition layers approximate Γ_t which move according to the volume-preserving mean curvature flow, Mullins–Sekerka flow and surface diffusion flow, respectively. First we use the energy functionals to show that the bulk energy is small comparing to the interfacial energy, then match the theoretical and numerical results to the geometric motions.

4.2.1. Interfacial motion: energy functionals

The dynamics of four equations tend to minimize energy, the shifting ϕ for moving interfaces can be estimated based on an energy argument. Let us assume that we have the Ginzburg–Landau functional

$$\mathcal{E} = \int_\Omega e(\phi) \, d\mathbf{x} = \int_\Omega \left(\frac{\epsilon}{2} |\nabla\phi|^2 + \frac{1}{\epsilon} F(\phi) \right) d\mathbf{x}$$

where e is the local free energy density of the system. Separating the functional $\mathcal{E}$ into an interfacial energy $\mathcal{E}_I$ and a bulk energy $\mathcal{E}_B$, the domain is divided by the bulk region where $|\phi^\epsilon| > 1 - \eta$ and the interfacial region where $|\phi^\epsilon| < 1 - \eta$ for small η. Then following inequality (20) holds from the work of Chen [25]. Thus, there exist positive constants C_0 and η_0 such that for every $\eta \in [0, \eta_0]$, every $\epsilon \in (0, 1]$, and every $(\phi^\epsilon, \mu^\epsilon)$,

$$\int_B [e^\epsilon(\phi^\epsilon)] \, d\mathbf{x} \le \int_B \left[e^\epsilon(\phi^\epsilon) + \frac{1}{\epsilon} f^2(\phi^\epsilon) \right] d\mathbf{x}$$

$$\le C_0\eta \int_I \epsilon|\nabla\phi^\epsilon|^2 \, d\mathbf{x} + C_0\epsilon \int_\Omega \mu^{\epsilon 2} \, d\mathbf{x} \le \int_I e^\epsilon(\phi^\epsilon) \, d\mathbf{x}. \quad (20)$$

We define $g(\phi)$ such that $g(\phi) = f(\phi)$ if $|\phi| \ge 1 - \eta$, $g(\phi) = 0$ if $|\phi| \le 1 - c_0$, and $g(\phi)$ is linear in the remaining part. The constant c_0 is defined by $f'(\phi) \ge |\phi|^{p-2}$ for some $p > 2$ if $|\phi| \ge 1 - c_0$. Then the identity holds

$$\int_\Omega \mu^\epsilon g(\phi^\epsilon) \, d\mathbf{x} = \int_\Omega \left[-\epsilon\Delta\phi^\epsilon + \frac{1}{\epsilon} f(\phi^\epsilon) \right] g(\phi^\epsilon) \, d\mathbf{x}$$

$$= \int_\Omega \left[\epsilon g'(\phi^\epsilon |\nabla\phi^\epsilon|^2) + \frac{1}{\epsilon} f(\phi^\epsilon) g(\phi^\epsilon) \right] d\mathbf{x}.$$

Using the Cauchy–Schwarz inequality,

$$\left| \int_\Omega \mu^\epsilon g(\phi^\epsilon) \, d\mathbf{x} \right| \le \int_\Omega \left[\frac{\epsilon}{2} \mu^{\epsilon 2} + \frac{1}{2\epsilon} g^2 \right] d\mathbf{x} \le \int_\Omega \left[\frac{\epsilon}{2} \mu^{\epsilon 2} + \frac{1}{2\epsilon} fg \right] d\mathbf{x}.$$

From the identity,

$$\int_\Omega \mu^\epsilon g(\phi^\epsilon) \, d\mathbf{x} = \int_\Omega \left[\epsilon g'(\phi^\epsilon |\nabla\phi^\epsilon|^2) + \frac{1}{\epsilon} f(\phi^\epsilon) g(\phi^\epsilon) \right] d\mathbf{x} \le \int_\Omega \frac{\epsilon}{2} \mu^{\epsilon 2} + \frac{1}{2\epsilon} fg \, d\mathbf{x}.$$

Then we separate the region Ω into the bulk region B and interfacial region I,

$$\int_B \left[\epsilon f'(\phi^\epsilon |\nabla\phi^\epsilon|^2) + \frac{1}{\epsilon} f^2(\phi^\epsilon) \right] d\mathbf{x} \le \int_B \left(\frac{\epsilon}{2} \mu^{\epsilon 2} + \frac{1}{2\epsilon} f^2 \right) d\mathbf{x} + \int_I \frac{\epsilon}{2} \mu^{\epsilon 2} \, d\mathbf{x} - \int_I \epsilon g'(\phi^\epsilon)|\nabla\phi^\epsilon|^2 \, d\mathbf{x}.$$

Since $F(\phi) \le Cf^2(\phi)$ when $|\phi| \ge 1 - c_0$, $|f(\pm(1-\eta))| = O(\eta)$, $g'(\phi) = O(\eta)$ when $|\phi| \le 1 - \eta$, we have

$$\int_B \left[e^\epsilon(\phi^\epsilon) + \frac{1}{\epsilon} f^2(\phi^\epsilon) \right] d\mathbf{x} \le C_0 \eta \int_I \epsilon |\nabla \phi^\epsilon|^2 \, d\mathbf{x} + C_0 \epsilon \int_\Omega \mu^{\epsilon 2} \, d\mathbf{x}.$$

Thus, we conclude that

$$\mathcal{E}_B \ll \mathcal{E}_I. \tag{21}$$

4.2.2. The circles case

Based on previous observations, we consider that the bulk energy is small comparing to the interfacial energy. For describing the motion of interface, we briefly explain how two circles evolve under the different equations. Suppose we have two circles with radii r_1 and r_2 such that $r_1 > r_2$ and enough long distance between them. The initial profile between two phases is assumed to impose the transition layer of the equations.

The model of the CAC1 equation represents energy decreasing for the energy functional

$$\mathcal{E}(\phi^\epsilon) = \int_\Omega \left(\frac{\epsilon}{2} |\nabla \phi^\epsilon|^2 + \frac{1}{\epsilon} F(\phi^\epsilon) \right) d\mathbf{x}, \tag{22}$$

we multiply Eq. (1) by $d\phi^\epsilon/dt$ and integrate with respect to $\mathbf{x}$.

$$\int_\Omega (\phi_t^\epsilon)^2 \, d\mathbf{x} = \int_\Omega \epsilon \Delta \phi^\epsilon \frac{d\phi^\epsilon}{dt} \, d\mathbf{x} - \int_\Omega \frac{1}{\epsilon} f(\phi^\epsilon) \frac{d\phi^\epsilon}{dt} \, d\mathbf{x} + \alpha(t) \int_\Omega \frac{d\phi^\epsilon}{dt} \, d\mathbf{x}.$$

This reduces to

$$\frac{d\mathcal{E}}{dt} = - \int_\Omega (\phi_t^\epsilon)^2 \, d\mathbf{x} \le 0.$$

The CAC2 equation follows with the same energy functional (22). Multiplying Eq. (2) by $\partial \phi^\epsilon / \partial t$ and integrating with respect to $\mathbf{x}$,

$$\int_\Omega \left(\frac{\partial \phi^\epsilon}{\partial t} \right)^2 d\mathbf{x} = \epsilon \int_\Omega \Delta \phi^\epsilon \frac{d\phi^\epsilon}{dt} \, d\mathbf{x} - \int_\Omega \frac{1}{\epsilon} f(\phi^\epsilon) \frac{\partial \phi^\epsilon}{\partial t} \, d\mathbf{x} + \beta \int_\Omega k(\phi^\epsilon) \frac{\partial \phi^\epsilon}{dt} \, d\mathbf{x}$$

$$= -\frac{d}{dt} \int_\Omega \left(\frac{\epsilon}{2} |\nabla \phi^\epsilon|^2 + \frac{1}{\epsilon} f(\phi^\epsilon) \right) d\mathbf{x} + \beta \frac{d}{dt} \int_\Omega K(\phi^\epsilon) \, d\mathbf{x},$$

we have

$$\frac{d\mathcal{E}}{dt} = - \int_\Omega (\phi_t^\epsilon)^2 \le 0.$$

Therefore the variation of the bulk energy for the CAC1 and CAC2 equations can be stated in the following way [89],

$$\delta \phi^\epsilon \approx -\frac{(2S_1 \delta r_1 + 2S_2 \delta r_2)}{|\Omega|} = -\frac{(4\pi r_1 \delta r_1 + 4\pi r_2 \delta r_2)}{|\Omega|},$$

where S_1 and S_2 are the perimeter of the two circles. Then bulk energy is uniformly changed

$$\delta \phi^\epsilon |\Omega| = \delta \mathcal{E}_B.$$

Under the constraint of mass-conservation and (21), the density distribution ϕ^ϵ of the bulk region transfers to interfacial region [62,67,89]. Thus, we have the following equations:

$$2\pi(r_1 + r_2) = 2\pi(r_1 + \delta r_1 - \delta r_A) + 2\pi(r_2 + \delta r_2 - \delta r_A)$$
$$\delta r_1 + \delta r_2 = 2\delta r_A.$$

where δr_1 and δr_2 are proportional to the reciprocal of the each circle's radius, and δr_A is the radius variation from the average of mean curvatures. Since $\delta r_2 \le \delta r_1$, we have

$$\delta r_1 - \delta r_A \le 0 \quad \text{and} \quad \delta r_2 - \delta r_A \ge 0.$$
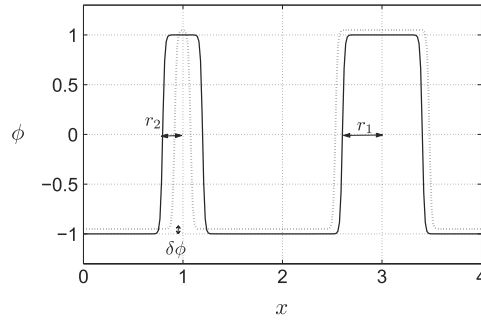
Fig. 4. Schematic plot of the shrinking and growing circles for the CAC1 and CAC2 equations.

Therefore, the radius r_1 increases, however r_2 decreases.

Fig. 4 illustrates the cross-sectional view of the CAC1 and CAC2 evolutions, and Fig. 5(a) and (b) show the evolutions in the computational domain Ω. If we assume that the interfaces of the CAC1 and CAC2 equations approximate the motion by the volume-preserving mean curvature flow, two circles' motion can be expected to move the following velocity:

$$\frac{dr_1}{dt} = \frac{1}{r_1} - \frac{2}{r_1 + r_2}$$
$$\frac{dr_2}{dt} = \frac{1}{r_2} - \frac{2}{r_1 + r_2}.$$

(23)

Eq. (23) also implies that the radius of the small one decreases but the big one increases.

Now we consider the CH and mCH equations. Multiplying (3) by μ and integrating over the domain Ω, we have energy decreasing inequality

$$\int_\Omega \mu \frac{\partial \phi^\epsilon}{\partial t} \, d\mathbf{x} = \int_\Omega \mu (\Delta \mu) \, d\mathbf{x}$$
$$\frac{d}{dt} \mathcal{E} = -\int_\Omega |\nabla \mu|^2 \, d\mathbf{x} \le 0.$$

The bulk energy for the CH equations remains small and diffuses since there are chemical potential and mobility $M \equiv 1$ in both regions. Therefore, even though the total energy is decreasing, shifting of the bulk ϕ^ϵ from the interfacial region occurs. It makes the bulk energy fluctuate from the steady state profile. This amounts to reduce the small circle's radius, and increase the big one's radius. To see this phenomenon, we recall that velocity of interface is given with chemical potential

$$V = \left[\frac{\partial \mu}{\partial n} \right]_{\Gamma_\tau} = \frac{\partial \mu^+}{\partial n} - \frac{\partial \mu^-}{\partial n} \quad \text{on } \Gamma_t.$$

Using this Mullins–Sekerka flow, the CH equations of the radii for r_1 and r_2 take the following forms [5]:

$$\frac{dr_1}{dt} = \frac{2}{|\log \varphi|} \frac{1}{r_1} \left(\frac{1}{\bar{r}} - \frac{1}{r_1} \right),$$
$$\frac{dr_2}{dt} = \frac{2}{|\log \varphi|} \frac{1}{r_2} \left(\frac{1}{\bar{r}} - \frac{1}{r_2} \right),$$

and the motion of the centers for ξ_1 and ξ_2,

$$\frac{d\xi_1}{dt} = \frac{-4}{|\log \varphi|} \left(\frac{1}{\bar{r}} - \frac{1}{r_2} \right) \frac{\xi_2 - \xi_1}{|\xi_2 - \xi_1|^2},$$
$$\frac{d\xi_2}{dt} = \frac{-4}{|\log \varphi|} \left(\frac{1}{\bar{r}} - \frac{1}{r_1} \right) \frac{\xi_1 - \xi_2}{|\xi_2 - \xi_1|^2},$$
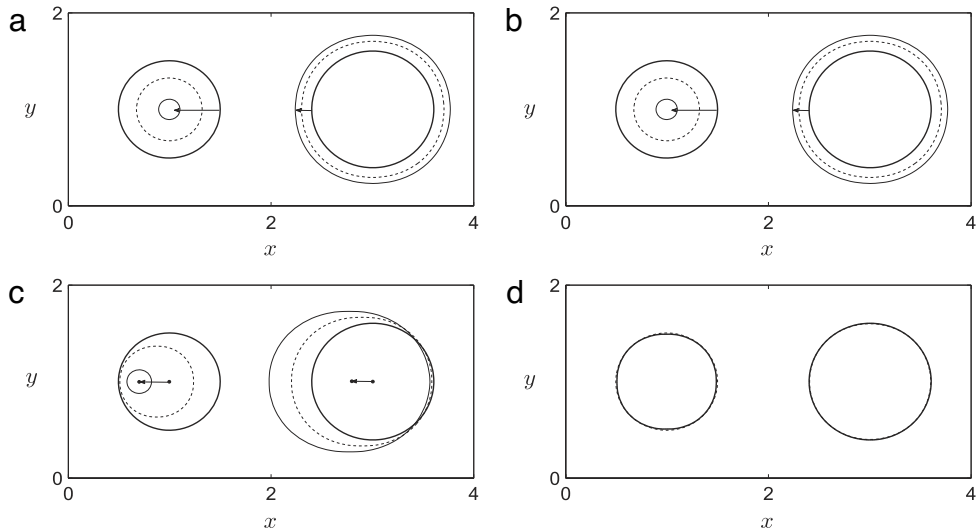
Fig. 5. (a) Evolutions under the CAC1 (a), CAC2 (b), CH (c) and mCH (d) equations. The horizontal axis is in space x and the vertical axis is in space y.

where φ is ratio between the volume of two circles and the domain $|\Omega|$

$$\varphi = \frac{|\Omega^-|}{|\Omega|} = \frac{\pi \left(r_1^2 + r_2^2\right)}{|\Omega|},$$

and $\bar{r}$ is the harmonic mean

$$\frac{1}{\bar{r}} = \frac{1}{2}\left(\frac{1}{r_1} + \frac{1}{r_2}\right).$$

Fig. 5(c) shows the evolutions under the CH equation. In this simulation, we see that the small circle becomes smaller and the big one becomes bigger, but the total area of the two circles is preserved. Meanwhile, the two centers of circles move to the left boundary.

For the mCH, we have

$$\int_\Omega \mu \frac{\partial \phi^\epsilon}{\partial t}\, d\mathbf{x} = \int_\Omega \mu \nabla(M(\phi^\epsilon)\nabla\mu)\, d\mathbf{x}$$
$$\frac{d}{dt}\mathcal{E} = -\int_\Omega M(\phi^\epsilon)|\nabla\mu|^2\, d\mathbf{x}$$

and, the time derivative of the energy functional can be written as

$$\frac{d}{dt}\mathcal{E}_B = 0,$$
$$\frac{d}{dt}\mathcal{E}_I = -\int_I M(\phi^\epsilon)|\nabla\mu|^2\, d\mathbf{x}$$

for η, ϕ^ϵ such that $M(\phi^\epsilon) \approx 0$, when $|\phi^\epsilon| > 1 - \eta$. Then the bulk energy for mCH equations is to be zero $\mathcal{E}_B \approx 0$ so that the variation of energy against time is none. Only interfacial energy decays locally until it reaches equilibrium. Once it forms a circle, the energy variation is none. This can be verified by the surface diffusion flow:

$$\frac{dr_1}{dt} = \Delta_s\left(\frac{1}{r_1}\right) = 0,$$
$$\frac{dr_2}{dt} = \Delta_s\left(\frac{1}{r_2}\right) = 0.$$

Therefore, no motion takes place on the interfaces of the two circles.
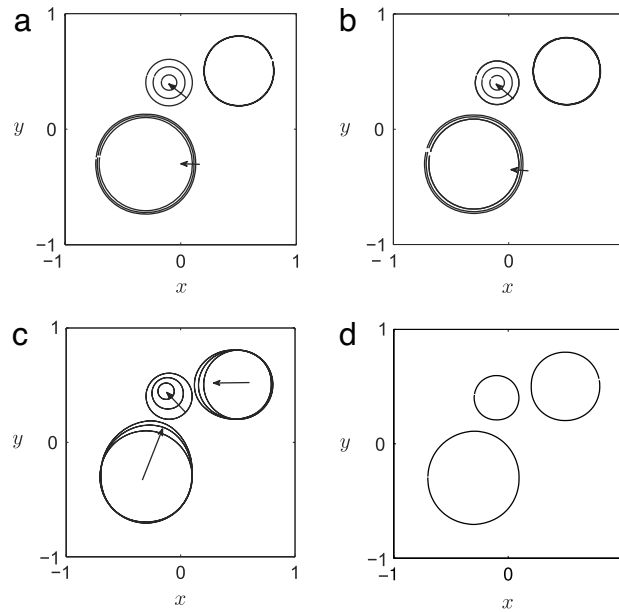
Fig. 6. The evolutions of the four equations. (a) CAC1, (b) CAC2, (c) CH, (d) mCH equations. The different size of circles are given.

For example, the initial profile is taken to be:

$$\phi(x, y, 0) = \tanh \frac{0.6 - \sqrt{(x - 1.0)^2 + (y - 1.0)^2}}{\sqrt{2}\epsilon_4} + \tanh \frac{0.5 - \sqrt{(x - 3.0)^2 + (y - 1.0)^2}}{\sqrt{2}\epsilon_4}$$

on the computational domain, $\Omega = (0, 4) \times (0, 2)$ with a 256×128 mesh grids. In this computation we use the parameter $h = 4/256$, $\Delta t = 0.025 \times h$ and ϵ_4.

Fig. 5 illustrates the evolutions under the CAC1 (a), CAC2 (b), CH (c), and the mCH (d) equations, respectively. In the evolutions under the CAC1, CAC2 and CH equations, the radius of the small circle decreases, and large one increases until small one vanishes. The difference of the dynamics is in that the radius of the large one driven by the CAC1 and CAC2 equations uniformly increases along the normal vector, since α and $\beta(t)$ are globally defined. On the other hand, the radius of the large one by the CH equations increases near to the small one. Thus, this makes the center of large one moves toward the small one.

In Fig. 6, we plot the zero-level set of the phase. The difference we can see is that the smaller circle shrinks in the evolutions of the CAC1, CAC2 and CH equations in common but the center of the smaller circle does not move in the dynamics of the CAC1 and CAC2 equations.

4.2.3. Small figure

Under the motions driven by the CAC1, CH and mCH equations, the circle shrinks throughout the evolutions. However the motion by the CAC2 equation allows to maintain its circle shape all the time (see Fig. 7). The asymptotic analysis in [15] suggested that the difference between the normal velocities V_n and V_n^{sharp} of diffuse and sharp interfaces is small in the CAC2 equation, i.e., $|V_n - V_n^{sharp}| < C\epsilon^2$, where the diffuse-interface approximates the sharp-interface. But the other conservative phase-field models [15,26] has approximation of $|V_n - V_n^{sharp}| < C\epsilon$ for some constant C.

In these numerical tests, a circle with radius 0.1 and center $(0.5, 0.5)$ on a domain $(0, 1) \times (0, 1)$ is taken as the initial condition:

$$\phi(x, y, 0) = \tanh \frac{0.1 - \sqrt{(x - 0.5)^2 + (y - 0.5)^2}}{\sqrt{2}\epsilon_n}.$$
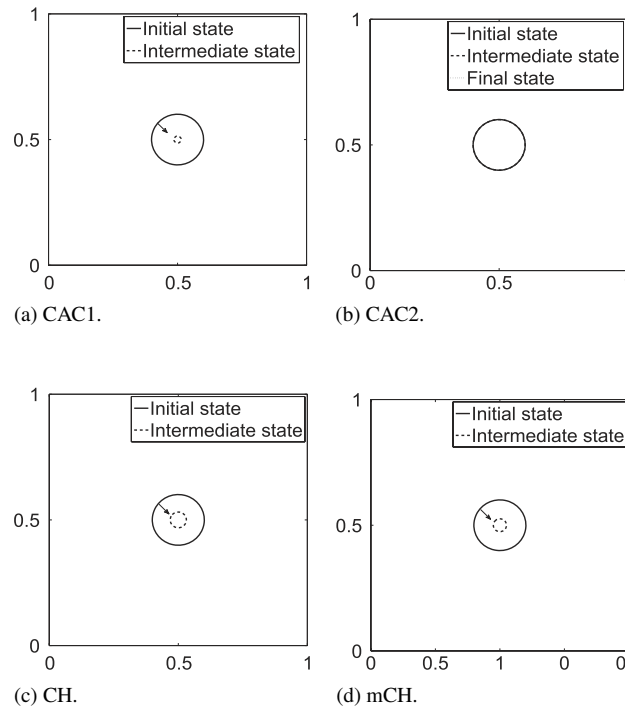
Fig. 7. Evolutions under the CAC1, CAC2, CH, and mCH equations. The horizontal axis is in space x and the vertical axis is in space y.
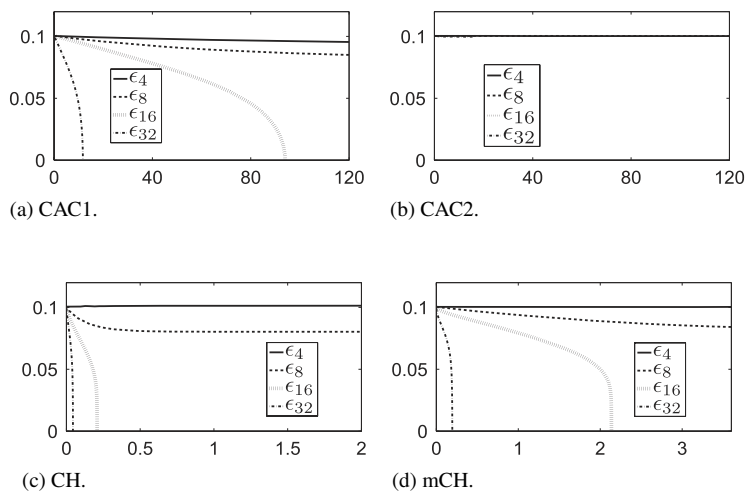
Fig. 8. Evolutions under the CAC1, CAC2, CH, and mCH equations. The horizontal axis is in time and the vertical axis is in radius.

Four different equations are evolved with spatial step size $h = 1/256$ and temporal step size $\Delta t = 0.025 \times h$ and we take the different epsilon values ϵ_n, $n = 4, 8, 16$, and 32. Fig. 8 shows the radius of diminishing circle at epsilon values ϵ_4, ϵ_8, ϵ_{16}, and ϵ_{32}. When we take epsilon values ϵ_{16} and ϵ_{32}, the circle disappears in evolutions, and it shrinks when we have ϵ_8. But we can observe the robustness of the CAC2 equation from the numerical tests (see Fig. 8(b)). Therefore we see that the approximation of the CAC2 equation has a better volume preserving property than the other conserving equations.
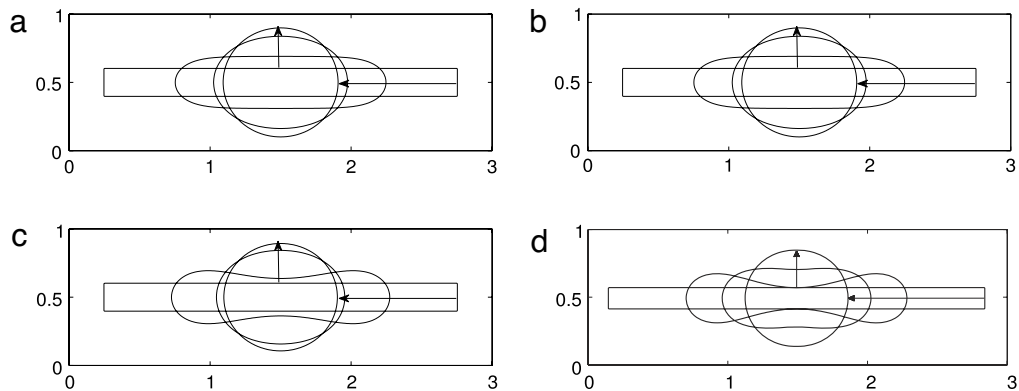
Fig. 9. Motion of capped off cylinders driven by the (a) CAC1, (b) CAC2, (c) CH and (d) mCH equations in two-dimensional space. The horizontal axis is in space x and the vertical axis is in space y.

4.3. Preserving the convexity

One of the distinguishing points among the CAC1, CAC2, CH and mCH equations is to preserve the convexity. The dynamics driven by the CH and mCH equations have no such property [32,44,52]. However, several mathematical and numerical analysis showed that the equation of the volume-preserving curvature flow preserves the convexity [41] when it has a convex curve given by the zero-level set of the solutions at the initial condition. Thus, the simple and convex curve evolved under the CAC1 equation, preserves the convexity due to its motion by volume-preserving mean curvature.

For the numerical test, the initial profile in two-dimensional space is chosen as

$$\phi(x, y, 0) = \begin{cases} 1 & \text{if } |x - 1.5| < 1.25, \ |y - 0.5| < 0.1, \\ -1 & \text{otherwise,} \end{cases}$$

on a domain Ω, $(0, 3) \times (0, 1)$. Numerical solutions are computed on 128×384 grids with $h = 1/128$, $\Delta t = 0.025 \times h$ and ϵ_4.

In Fig. 9, we show the evolutions with four different equations in two-dimensional space. Four models are contrasted with volume-preserving mean curvature flow where convexity is preserved in convex shape [41]. The loss of convexity in the Mullins–Sekerka flow and surface diffusion flow reflects that the fourth order parabolic approximated by the CH and mCH equations does not fulfill the comparison principle which is main property of a second order parabolic equation. As we can see, the convex curves enclosed zero-level set of the CAC1 and CAC2 equations' solutions stay convex. However, the curves of the CH and mCH equations do not hold it. It was also shown by Mayer [64] that the Mullins–Sekerka flow does not preserve convexity in two-dimensional space.

4.4. Non-convex case

Now consider the initial curve, which is simple and closed, that contains the long and parallel bars, (see Fig. 10). The domain is selected to be the $(0, 4) \times (0, 2)$ with $Nx = 512$ and $Ny = 256$ grid points. We take ϵ_4, $h = 1/256$, and $\Delta t = 0.025 \times h$. For the initial conditions, we put a small circle centered at $(0.78, 1)$ with a radius 0.55, and construct two thick bars having gap 0.16 between each others as well as boundary of the domain and the bars, respectively.

The curves of the CAC1 and CAC2 equations evolve without making any hole, whereas the curves of the CH and mCH equations stick together during the evolutions. The formed hole of the CH equation is smaller than the one of the mCH equation, since the curve under the CH equations moves and shrinks by the Mullins–Sekerka flow. Note that for the volume preserving mean curvature flow the numerical examples showed that the curves evolved under AC1
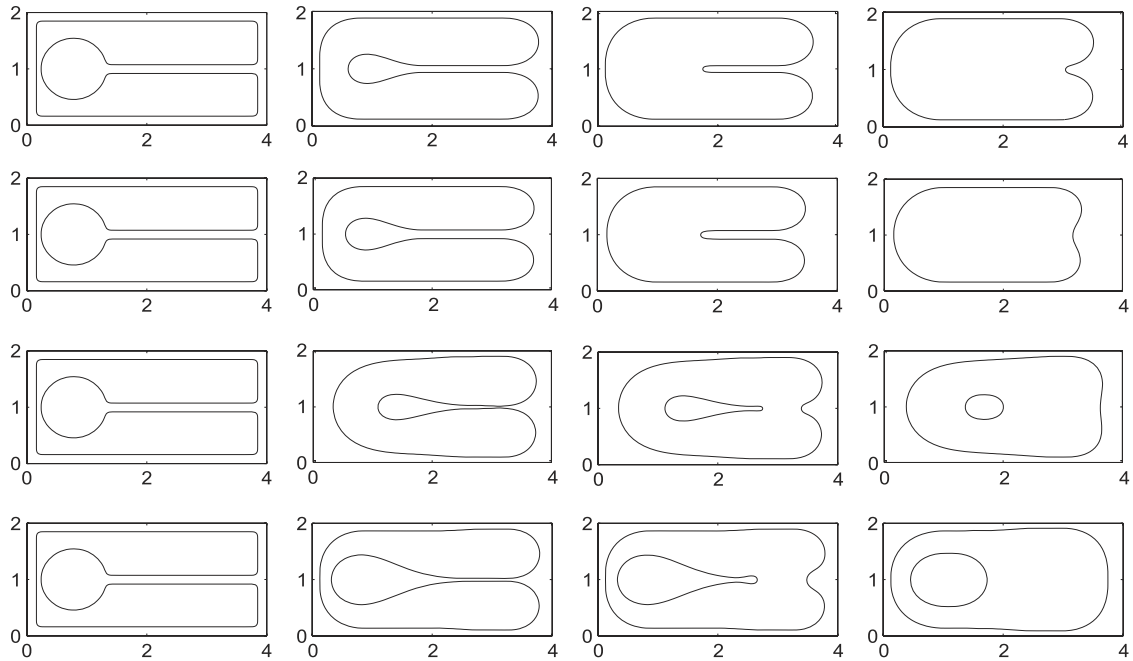
Fig. 10. Motion driven by the CAC1 (first row), CAC2 (second row), CH (third row) and mCH (fourth row) equations in two-dimensional space. The horizontal axis is in space x and the vertical axis is in space y.

and CAC2 equations also may not preserve convexity [65] and have self-intersections [66]. In this case we emphasize only the difference in the four-conservative models by setting the initial condition.

4.5. Long time behaviors of the solutions

In the longer time behaviors of four equations, the phases converge to situations where each phase occupies one connected part of the domain. Here we consider the long-time behaviors of the four equations. The behavior of the phase-field equations is to minimize the value of $E(\phi)$, which implies that the zero-level set of the solutions approaches to critical values. Thus, steady state solutions of conservative equations converge to the solution of the isoperimetric problem. Thus, these equations can be used to generate constant mean curvature (CMC) surfaces that minimize interfacial area subject to a volume constraint. When it has the equal volume fraction of the two components, the interface forms minimal surfaces.

We presented three dimensional simulations. Even though statistical studies of solutions depend on the initial value and boundary conditions, there is a geometric meaning for the isoperimetric problem [28,45]. Thus, the global minimized surfaces such as sphere, cylinder, plane, CMC and minimal surfaces are obtained for the prescribed volume fraction. The numerical tests with random initial conditions were performed in section.

We perform numerical simulations of the conservative phase-field equations with constant volume fractions $\bar{\phi} = 0.0$ and $\bar{\phi} = -0.5$ where we denote $\bar{\phi}$ by the difference of the volume fraction of each phase. The CAC1, CAC2, CH, and mCH equations conserve the volume fraction in the dynamics, but the interface of the phases moves differently with the same initial data. In this tests, we prescribe the difference of the volume fraction at the initial time. Thus we give the random number with mean $\bar{\phi} = 0.0$ and $\bar{\phi} = -0.5$. Fig. 11 illustrates the zero-level contour of phases at the initial time.

In the figures from 12 to 15, we give numerical contour plots of the phases. The first row at each figure represents the difference of the volume fraction $\bar{\phi} = 0.0$, and second row implies that $\bar{\phi} = -0.5$, respectively. Also the first column at each figure shows the intermediate evolutions, and the second column corresponds to the numerical steady state.
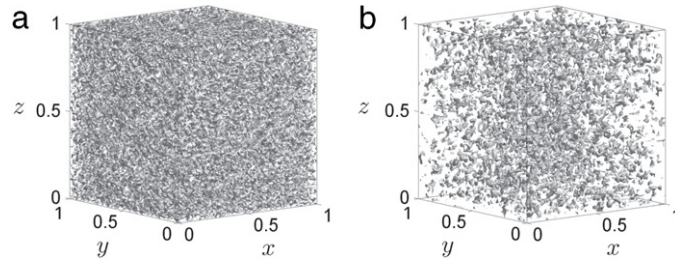
Fig. 11. Initial data with (a) $\bar{\phi} = 0.0$ and (b) $\bar{\phi} = -0.5$.
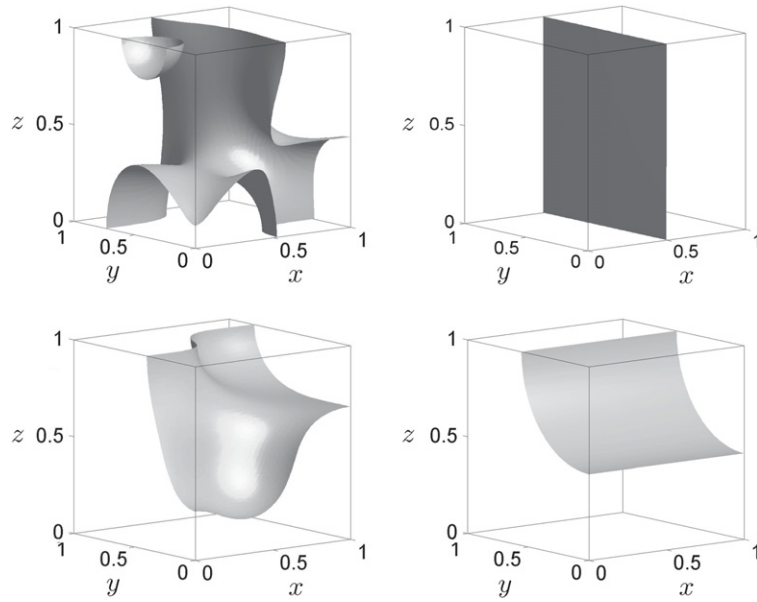
Fig. 12. CAC1.
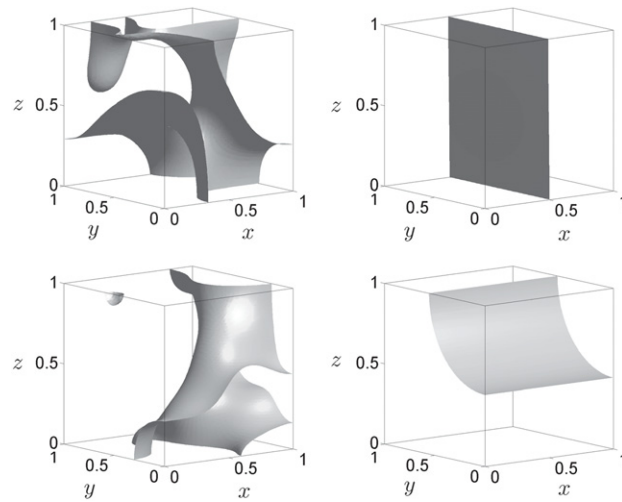
Fig. 13. CAC2.
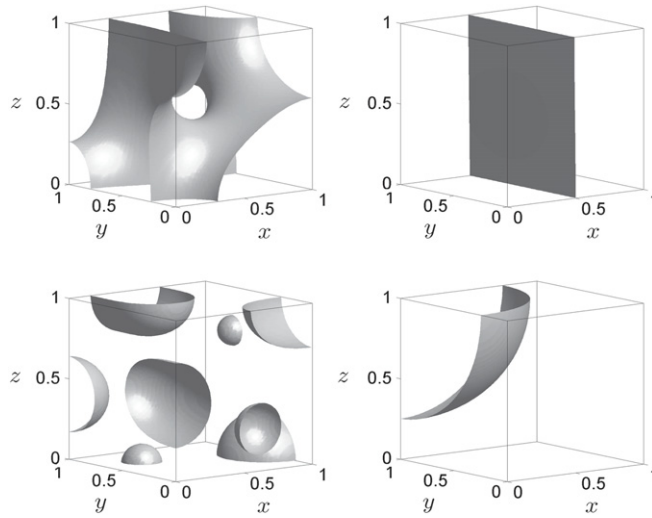
Fig. 14. CH.
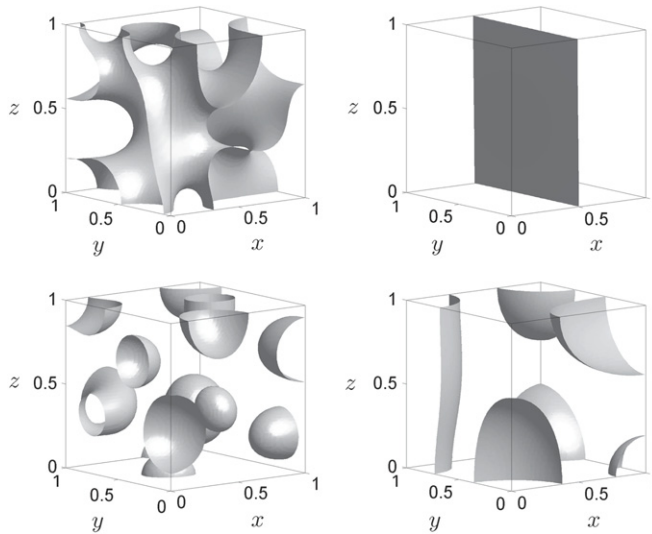
Fig. 15. mCH.

4.6. Convergence test

The convergence of the method by refinements were performed in [30,53,55,86]. We also observe the convergence tests on a domain $\Omega = (0, 1) \times (0, 1)$. The initial data is given by

$$\phi(x, y) = 0.15 \cos(\pi x) \cos(2\pi y) + 0.3 \cos(3\pi x) \cos(\pi y).$$

The numerical solutions are approximated on the uniform grids, $h = 1/2^n$ for $n = 5, 6, 7$, and 8. For each test, the calculation is run up to time $T = 0.0001$ with the uniform temporal step size, $\Delta t = 0.1h^2$ and $\epsilon = 0.01$. Now we define the l_2-norm error of a grid, which is founded in finer mesh grid. The error of the difference between grid and the average of the next finer grid cells is defined by

$$e_{h/\frac{h}{2}ij} := \phi_{hij} - (\phi_{\frac{h}{2}2i,2j} + \phi_{\frac{h}{2}2i-1,2j} + \phi_{\frac{h}{2}2i,2j-1} + \phi_{\frac{h}{2}2i-1,2j-1})/4.$$

Then the ratio of successive error is defined as follows $\log_2(\|e_{h/\frac{h}{2}}\|/\|e_{\frac{h}{2}/\frac{h}{4}}\|)$. The mesh refinement convergence results with $\Delta t = h^2$ are given in Table 1.

Table 1
Convergence test.

CAC1	32−64	Rate	64−128	Rate	128−256
l_2	9.257e−04	2.004	2.308e−04	1.999	5.773e−04
CAC2	32−64	Rate	−64−128	Rate	128−256
l_2	9.257e−04	2.004	2.308e−04	1.999	5.773e−04
CH	32−64	Rate	64−128	Rate	128−256
l_2	9.019e−04	2.414	1.693e−04	2.003	4.224e−05
mCH	32−64	Rate	64−128	Rate	128−256
l_2	9.014e−04	2.411	1.695e−04	2.003	4.228e−05

5. Conclusions

In this paper, a comparison study of the conservative Allen–Cahn and the Cahn–Hilliard equations was theoretically and numerically performed. The equations were discretized by using finite difference schemes, and then the discrete systems of equations were solved using a nonlinear multigrid method. We presented the geometric flows, and matched them to the numerical experiments which highlight different dynamics of the four equations. Even though we could not study the physical meaning of the each equation, we demonstrated the characterizations for generation of interface and motion of interface. In particular, we showed that the constant and variable Cahn–Hilliard equations cannot remain a convex initial interface, while the conservative and modified Allen–Cahn equations keep the convex curve of the zero-level set with global mass correction, so that there is no self-intersection. With the property of mass-conservation and the behaviors of the solutions, these conservative phase-field models will be widely applied in simulating the fluid dynamics.

References

[1] S. Aland, J. Lowengrub, A. Voigt, Two-phase flow in complex geometries: A diffuse domain approach, Comput. Model. Eng. Sci. 57 (2010) 77–108.
[2] M. Alfaro, Generation, motion and thickness of transition layers for a nonlocal Allen—Cahn equation, Nonlinear Anal. Theor. 72 (2010) 3324–3336.
[3] M. Alfaro, D. Hilhorst, Generation of interface for an Allen–Cahn equation with nonlinear diffusion, Math. Model. Nat. Phenom. 5 (2010) 1–12.
[4] N.D. Alikakos, P.W. Bates, X. Chen, Convergence of the Cahn–Hilliard equation to the Hele-Shaw model, Arch. Ration. Mech. Anal. 128 (1994) 165–205.
[5] N.D. Alikakos, G. Fusco, G. Karali, Ostwald ripening in two dimensions the rigorous derivation of the equations from the Mullins–Sekerka dynamics, J. Differential Equations 205 (2004) 1–49.
[6] N.D. Alikakos, W.R. McKinney, in: K.J. Brown, A.A. Lacey (Eds.), Reation-Diffusion Equations: Remarks on the Equilibrium Theory for the Cahn–Hilliard in One Space Dimension, Oxford Science Publications, New York, 1993, pp. 75–93.
[7] M. Argentina, M.G. Clerc, R. Rojas, E. Tirapegui, Coarsening dynamics of the one-dimensional Cahn–Hilliard model, Phys. Rev. E 12 (2005) 1–15.
[8] M. Athanassenas, Volume-preserving mean curvature flow of rotationally symmetric surfaces, Comment. Math. Helv. 72 (1997) 52–66.
[9] F. Bai, A. Spence, A.M. Stuart, Numerical computations of coarsening in the one-dimensional Cahn–Hilliard model of phase separation, Physica D 78 (1994) 155–165.
[10] J.W. Barrett, J.F. Blowey, Finite element approximation of an Allen–Cahn/Cahn–Hilliard System, IMA J. Numer. Anal. 22 (2002) 11–71.
[11] P.W. Bates, S. Brown, J. Han, Numerical analysis for a nonlocal Allen–Cahn equation, Int. J. Numer. Anal. Model. 6 (2009) 33–49.
[12] P.W. Bates, P.C. Fife, Dynamics of nucleation for the Cahn–Hilliard equation, SIAM. J. Appl. Math. 53 (1993) 990–1008.
[13] M. Beneš, S. Yazaki, M. Kimura, Computational studies of non-local anisotropic Allen–Cahn equation, Math. Bohem. 4 (2011) 429–437.
[14] A. Bertia, I. Bochicchiob, A mathematical model for phase separation: A generalized Cahn–Hilliard equation, Math. Methods Appl. Sci. 34 (2011) 1193–1201.

[15] M. Brassel, E. Bretin, A modified phase-field approximation for mean curvature flow with conservation of the volume, Math. Methods Appl. Sci. 34 (2011) 1157–1180.
[16] W.L. Briggs, A Multigrid Tutorial, SIAM, Philadelphia, 1987.
[17] L. Bronsard, B. Stoth, Volume-preserving mean curvature flow as a limit of a nonlocal Ginzburg-Landau equation, SIAM J. Math. Anal. 28 (1997) 769–807.
[18] G. Caginalp, Phase field models and sharp interface limits: some differences in subtle situations, Rocky Mountain J. Math. 27 (1991) 603–615.
[19] J.W. Cahn, On spinodal decomposition, Acta Met. 9 (1961) 795–801.
[20] J.W. Cahn, C.M. Elliott, A. Novick-Cohen, The Cahn–Hilliard equation with a concentration dependent mobility: motion by minus the Laplacian of the mean curvature, European J. Appl. Math. 7 (1996) 287–301.
[21] J.W. Cahn, J.E. Hilliard, Free energy of a non-uniform system, I. Interfacial free energy, J. Chem. Phys. 28 (1958) 258–267.
[22] J.W. Cahn, A. Novick-Cohen, The Cahn–Hilliard with a concentration dependent mobility: motion by minus the Laplacian of the mean curvature, European J. Appl. Math. 7 (1996) 287–301.
[23] E.A. Carlen, M.C. Carvalho, E. Orlandi, Approximate solutions of the Cahn–Hilliard equation via corrections to the Mullins–Sekerka motion, Arch. Ration. Mech. Anal. 178 (2005) 1–55.
[24] X. Chen, The Hele-Shaw problem and area-preserving curve-shortening motions, Arch. Ration. Mech. Anal. 123 (1993) 117–151.
[25] X. Chen, Global asymptotic limit of solutions of the Cahn–Hilliard equation, J. Differential Geom. 44 (1996) 262–311.
[26] X. Chen, G. Caginalp, A rapidly converging phase-field model, Discrete Contin. Dyn. Syst. 15 (2006) 1017–1034.
[27] X. Chen, C.M. Elliott, A. Gardiner, J.J. Zhao, Convergence of numerical solutions to the Allen–Cahn equation, Appl. Anal. 69 (1998) 47–56.
[28] R. Choksi, P. Sternberg, Periodic phase separation: the periodic Cahn–Hilliard and isoperimetric problems, Interfaces Free Bound. 8 (2006) 371–392.
[29] S.M. Choo, S.M. Chung, Y.J. Lee, Conservative nonlinear difference scheme for the Cahn–Hilliard equationII, Comput. Math. Appl. 39 (2000) 229–243.
[30] A. Christlieb, J. Jones, K. Promislow, B. Wetton, M. Willoughby, High accuracy solutions to energy gradient flows from material science models, J. Comput. Phys. 257 (2014) 193–215.
[31] A. Christlieb, K. Promislow, Z. Xu, On the unconditionally gradient stable scheme for the Cahn–Hilliard equation and its implementation with Fourier method, Commun. Math. Sci. 11 (2013) 345–360.
[32] B.D. Coleman, R.S. Falk, M. Moakher, Stability of cylindrical bodies in the theory of surface diffusion, Physica D 89 (1995) 123–135.
[33] S. Dai, Q. Du, Motion of interfaces governed by the Cahn–Hilliard equation with highly disparate diffusion mobility, SIAM J. Appl. Math. 72 1818–1841.
[34] M. Do-Quang, G. Amberg, Numerical simulation of the coupling problems of a solid sphere impacting on a liquid free surface, Math. Comput. Simul. 80 (2010) 1664–1673.
[35] C.M. Elliott, in: J.F. Rodrigues (Ed.), Mathematical Models for Phase Change Problems: The Cahn–Hilliard Model for the Kinetics of Phase Separation, Birkhäuser, 1989, pp. 35–73.
[36] C.M. Elliott, H. Garcke, On the Cahn–Hilliard equation with degenerate mobility, SIAM J. Math. Anal. 27 (1996) 404–423.
[37] J. Escher, U.F. Mayer, G. Simonett, The surface diffusion flow for immersed hypersurfaces, SIAM J. Math. Anal. 29 (1998) 1419–1433.
[38] J. Escher, G. Simonett, Classical solutions for Hele-Shaw models with surface tension, Adv. Differential Equations 2 (1997) 619–642.
[39] D.J. Eyre, Unconditionally gradient stable time marching the Cahn–Hilliard equation, in: Computational and Mathematical Moels of Microstrucural Evolution, in: Mater. Res. Soc. Sympos. Proc., vol. 529, San Francisco, CA, 1998 pp. 39–46.
[40] X. Feng, A. Prohl, Numerical analysis of the Allen–Cahn equation and approximation for mean curvature flows, Numer. Math. 94 (2003) 33–65.
[41] M. Gage, On an area preserving evolution equation for plane curves, in: Nonlinear Problems in Geometry, in: Contemp. Math., vol. 51, 1986, pp. 51–62.
[42] H. Garcke, B. Nestler, B. Stinner, F. Wendler, Allen–Cahn systems with volume constraints, Math. Models Methods Appl. Sci. 18 (2008) 1347–1381.
[43] I.M. Gelfand, S.V. Fomin, Calculus of Variations, Dover Publications, INC, Mineola, New York, 1987.
[44] Y. Giga, K. Ito, Loss of convexity of simple closed curves moved by surface diffusion, Prog. Nonlinear Differ. Equ. Appl. 35 (1999) 305–320.
[45] H. Gómez, V.M. Calo, Y. Bazilevs, J.R. Hughes, Isogeometric analysis of the Cahn–Hilliard phase-field model, Comput. Methods Appl. Mech. Engrg. 197 (2008) 4333–4352.
[46] C.P. Grant, Spinodal decomposition for the Cahn–Hilliard equation, Comm. Partial Differential Equations 18 (1993) 453–490.
[47] M.E. Gurtin, G.B. McFadden, On the Evolution of Phase Boundaries, in: The IMA Volumes in Mathematics and its Applications, Springer, Oxford, 1993.
[48] F. Haußer, S. Rasche, A. Voigt, The inuence of electric elds on nanostructures—simulation and control, Math. Comput. Simul. 80 (2010) 1449–1457.
[49] P. Howard, Spectral analysis of stationary solutions of the Cahn–Hilliard equation, Adv. Differential Equations 14 (2009) 87–120.
[50] P. Howard, Spectral analysis of stationary solutions of the Cahn–Hilliard equation in $\mathbb{R}^d$, Comm. Partial Differential Equations 35 (2010) 590–612.
[51] G. Huisken, The volume preserving mean curvature flow, J. Reine Angew. Math. 382 (1987) 35–48.
[52] K. Ito, The surface diffusion flow does not preserve the convexity, RIMS Kôkyûroku Bessatsu 1105 (1999) 10–21.
[53] J. Kim, A numerical method for the Cahn–Hilliard equation with a variable mobility, Commun. Nonlinear Sci. Numer. Simul. 12 (2007) 1560–15711.
[54] J. Kim, Phase-field models for multi-component fluid flows, Commun. Comput. Phys. 12 (2012) 613–661.
[55] K. Kim, K. Kang, J. Lowengrub, Conservative multigrid methods for Cahn–Hilliard fluids, J. Comput. Phys. 193 (2004) 511–543.
[56] J. Kim, J. Lowengrub, Conservative multigrid methods for Cahn–Hilliard fluids, J. Comput. Phys. 193 (2004) 511–543.
[57] H.B. Lawson, Lectures on Minimal Submanifolds, Publisch or Persih, Berkeley, 1980.

[58] H. Lee, J.Y. Lee, A semi-analytical Fourier spectral method for the Allen–Cahn equation, Comput. Math. Appl. 68 (2014) 174–184.
[59] W. Liu, A.L. Bertozzi, T. Kolokolnikov, Diffuse interface surface tension models in an expanding flow, Commun. Math. Sci. 10 (2012) 387–418.
[60] F. Liu, J. Shen, Stabilized semi-implicit spectral deferred correction methods are constructed for the time discretization of Allen–Cahn and Cahn–Hilliard equations, Math. Methods Appl. Sci. 2013 (2013) 1–11.
[61] J. Lowengrub, L. Truskinovsky, Quasi-incompressible Cahn–Hilliard fluids and topological transitions, Proc. R. Soc. Lond. Ser. A 454 (1998) 2617–2654.
[62] S. Luckhaus, L. Modica, The Gibbs-Thompson relation within the gradient theory of phase transitions, Arch. Rational Mech. Anal. 27. VII. 107 (1989) 71–83.
[63] S. Maier-Paape, B.E. Moore, E.S. van Vleck, Spinodal decomposition for spatially discrete Cahn–Hilliard equations, Dyn. Contin. Discrete I 12 (2005) 529–554.
[64] U.F. Mayer, Two-sided Mullins–Sekerka flow does not preserve convexity, Electron. J. Differential Equations 1997 (1997) 171–179.
[65] U.F. Mayer, A numerical scheme for moving boundary problems that are gradient flows for the area functional, European J. Appl. Math. 11 (2000) 61–80.
[66] U.F. Mayer, G. Simonett, Self-intersections for the surface diffusion and the volume-preserving mean curvature flow, Differential Integral Equations 13 (2000) 118–1199.
[67] L. Modica, The gradient theory of phase transitions and the minimal interface criterion, Arch. Rational Mech. Anal. 6. VII. 98 (1987) 123–142.
[68] W.W. Mullins, Theory of thermal grooving, J. Appl. Phys. 28 (1957) 333–339.
[69] A. Novick-Cohen, The Cahn–Hilliard equation: Mathematical and modeling perspectives, Adv. Math. Sci. Appl. 8 (1998) 965–985.
[70] A. Novick-Cohen, in: C.M. Dafermos, M. Pokorny (Eds.), Handbook of Differential Equations: Evolutionary Equations 4, in: The Cahn–Hilliard Equation, Elsevier, 2008, pp. 201–228.
[71] A. Novick-Cohen, L.P. Hari, Geometric motion for a degenerate Allen–Cahn/Cahn–Hilliard system: The partial wetting case, Physica D 209 (2005) 205–235.
[72] R.L. Pego, Front migration in the nonlinear Cahn–Hilliard equation, Proc. R. Soc. Lond. Ser. A 422 (1989) 261–278.
[73] J. Rubinstein, P. Sternberg, Nonlocal reaction–diffusion equations and nucleation, IMA. J. Appl. Math. 48 (1992) 249–264.
[74] S.J. Ruuth, B.T.R. Wetton, A simple scheme for volume-preserving motion by mean curvature, J. Sci. Comput. 19 (2003) 373–384.
[75] J. Shen, X. Yang, A phase-field model and its numerical approximation for two-phase incompressible flows with different densities and viscosities, SIAM J. Sci. Comput. 32 (2010) 1159–1179.
[76] J. Shen, X. Yang, Numerical approximations of Allen–Cahn and Cahn–Hilliard equations, Discrete Contin. Dyn. Syst. 28 (2010) 1669–1691.
[77] D.N. Sibley, A. Nold, N. Sawa, S. Kalliadasis, The contact line behaviour of solid–liquid–gas diffuse-interface models, Phys. Fluids 25 (2013) 1–27.
[78] B.E.E. Stoth, Convergence of the Cahn–Hilliard equation to the Mullins–Sekerka problem in spherical symmetry, J. Differential Equations 125 (1996) 154–183.
[79] N. Takada, M. Misawa, A. Tomiyama, A phase-eld method for interface-tracking simulation of two-phase ows, Math. Comput. Simul. 72 (2010) 220–226.
[80] Z. Tan, K.M. Lim, B.C. Khoo, An adaptive mesh redistribution method for the incompressible mixture flows using phase-field model, J. Comput. Phys. 225 (2007) 1137–1158.
[81] U. Trottenberg, C. Oosterlee, A. Schuller, Multigrid, Academic Press, London, 2001.
[82] S.R. Upresti, Optimal Control for Chenmical Engineers, CRC Press, 2013.
[83] L. Vanherpe, F. Wendler, B. Nestler, S. Vandewalle, A multigrid solver for phase eld simulation of microstructure evolution, Math. Comput. Simul. 80 (2010) 1438–1448.
[84] M.J. Ward, Metastable bubble solutions for the Allen–Cahn equation with mass conservation, SIAM J. Appl. Math. 56 (1996) 1247–1279.
[85] G. Wheeler, Surface diffusion flow near spheres, Calc. Var. Partial Differential Equations 44 (2012) 131–151.
[86] M.R. Willoughby, High-order time adaptive numerical methods for the Allen–Cahn and Cahn–Hilliard equations (M.Sc. thesis), The University of British Columbia, 2011, December.
[87] S.M. Wise, C. Wang, J. Lowengrub, An energy-stable and convergent finite-difference scheme for the phase-field crystal equation, SIAM J. Numer. Anal. 47 (2009) 2269–2288.
[88] X. Yang, Error analysis of stabilized semi-implicit method of Allen–Cahn equation, Discrete Contin. Dyn. Syst. Ser. B 11 (2009) 1057–1070.
[89] P. Yue, C. Zhou, J.J. Feng, Spontaneous shrinkage of drops and mass conservation in phase-field simulations, J. Comput. Phys. 223 (2007) 1–9.
[90] J. Zhang, Q. Du, Numerical studies of discrete approximations to the Allen–Cahn equation in the sharp interface limit, SIAM J. Sci. Comput. 34 (2009) 3042–3063.
[91] J. Zhu, L.Q. Chen, J. Shen, V. Tikare, Coarsening kinetics from a variable-mobility Cahn–Hilliard equation: application of a semi-implicit Fourier spectral method, Phys. Rev. E 60 (1999) 3564–35723.